JACS
JOURNAL OF THE AMERICAN CHEMICAL SOCIETY
Article
pubs.acs.org/JACS

A Theoretical Investigation on the Mechanism and Stereochemical Course of the Addition of (*E*)-2-Butenyltrimethylsilane to Acetaldehyde by Electrophilic and Nucleophilic Activation

Larry M. Wolf and Scott E. Denmark*

Roger Adams Laboratory, Department of Chemistry, University of Illinois, Urbana, Illinois 61801, United States

Supporting Information

ABSTRACT: The diastereoselectivity of the addition of (*E*)-2-butenyltrimethylsilane to acetaldehyde under electrophilic (BF_3, H_3O^+) and nucleophilic (F^-) activation is investigated using density functional theory (M06-2X). The interaction–distortion/activation–strain model of reactivity is used to rationalize the origin of the selectivity. Consistent with experimental model systems, the synclinal transition states are determined to be preferred over the antiperiplanar transition states in the electrophilic-activated manifolds and vice versa for the fluoride-activated manifold. The selectivity for the syn diastereomer in the electrophilic activation manifolds is accounted for by increased electrostatic and orbital interactions for a synclinal transition state (**syn-T3**) at the expense of increased steric interactions relative to antiperiplanar transition states. The enhanced orbital interactions for the synclinal (**syn-T3**) versus antiperiplanar transition states can be attributed to increased $\pi \rightarrow \pi^*$ interactions. The selectivity for the anti diastereomer in the nucleophilic manifold is explained by the lesser electrostatic repulsion in the antiperiplanar transition states which are favored relative to the synclinal transition states. Additionally, the diastereoselectivity is partly attributed to variation in the distortion of the crotylsilane.

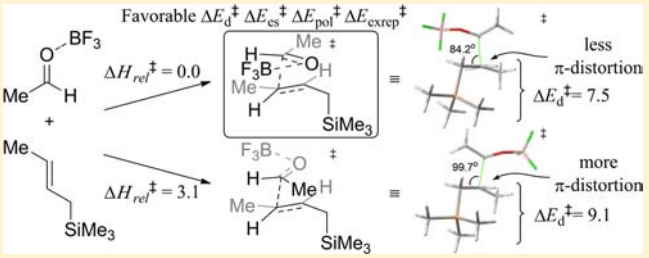

1. INTRODUCTION

The controlled construction of contiguous stereocenters is of primary importance in the synthesis of natural and non-natural products. A significant number of methods developed for this purpose involve the combination of two π systems, specifically those of electron-rich alkenes with aldehydes and ketones. The stereochemical course of the bond-forming event is dictated by the relative topicity of prostereogenic carbons in the transition state (Scheme 1). Each pairwise combination leads to a unique stereoisomer, for which three, limiting, staggered arrangements of the double bonds are possible: antiperiplanar, (+)-synclinal, and (−)-synclinal. The ability to *reliably* predict the stereochemical outcome of such reactions is vital for synthetic planning and requires an understanding of the physical origins underlying the way in which the structural and electronic properties of the two π systems (A, D, R^1, R^2) influence their relative orientations in the competing transition structures. Effective stereocontrol mechanisms often rely on strong organizational elements that enforce propinquity of the reacting components, such as metal coordination or dative association with directing groups. On the other hand, some of the most challenging reactions to rationalize are typically those that are believed to proceed through open transition-state structures, in which selectivity controlling factors pertain primarily to nonbonding interactions. Such reactions are the focus of this study.

An early phenomenological analysis of the stereochemical course of these types of reactions formulated a set of topological rules,[1] which are summarized here because they will be referred to frequently in the following sections (Scheme 2): (i) All vicinal bonds are staggered; (ii) a synclinal arrangement of the donor (C═D) and acceptor (C═A)

Scheme 1

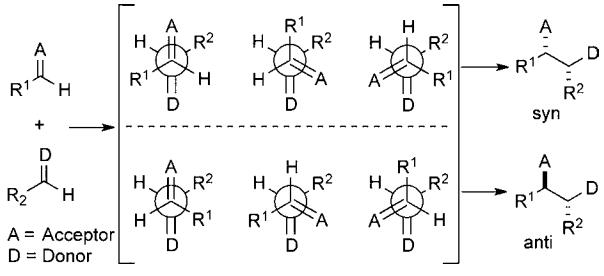

Scheme 2

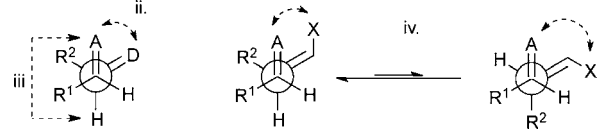

Received: December 8, 2012
Published: March 13, 2013

dx.doi.org/10.1021/ja311889v | *J. Am. Chem. Soc.* 2013, 135, 4743–4756

bonds is preferred; (iii) the smaller group on the donor (H) is placed antiperiplanar with respect to the C═A bond; and (iv) the synclinal orientation adopted is that which positions the donor and acceptor atoms in the closest possible proximity. Rules (i) and (iii) address the minimization of steric interactions, whereas rules (ii) and (iv) have electronic implications. Rule ii has received the most scrutiny experimentally.

A host of interactions have been suggested to explain these preferences, including minimization and/or maximization of unlike and like charge separation, respectively (Coulombic),[2] steric effects,[3] orbital control,[4] and dispersion forces.[5] However, the dominant selectivity controlling interactions that are related to the structure of the π systems still remains unclear. Each of the suggested effects is to some extent associated with the components of the interaction energy of the two fragments in the transition state. The aim of this investigation was to computationally identify the interactions that are most accountable for the diastereoselective preference in pathways thought to proceed through open transition states using theoretical methods.

The addition of electron-rich π systems to activated carbonyl groups constitutes a large body of reactions.[6] The stereochemical course of these reactions is often highly predictable through the use of cyclic transition-state models. Conversely, a physical understanding of stereochemical control in acyclic transition structures is less well developed. However, this has not prevented the accumulation of substantial amounts of experimental data that have allowed for the formulation of rules and generalities that possess some qualitative predictive capacity.[7] The immense synthetic utility of the addition of allylsilanes to aldehydes made it ideally suited to serve as the platform for this study.

2. BACKGROUND

2.1. Experimental Studies. Beyond the edifice of preparative studies on the Lewis acid-mediated addition of allylsilanes to aldehydes, the reaction mechanism and stereochemical course have been extensively investigated. Thorough stereochemical studies have established that the reaction of allylic trialkylsilanes proceeds through acyclic (open) transition states (Scheme 3).[8] This behavior is in contrast to the reactions of allylboron reagents that proceed through closed transition states because of the Lewis acidic nature of the tricoordinate boron atom.[9] Consequently, six limiting transition structures can be envisioned that possess staggered orientations of all bonds to minimize steric interactions (rule i). Additionally, the Lewis acid is coordinated to the aldehyde oxygen on the side of the hydrogen atom, as has been amply demonstrated in spectroscopic and computational studies.[10] The silicon group and the electrophile are located on opposite sides of the allyl moiety (i.e., anti S_E2') which established the open nature of the transition state.[8] A syn disposition (established for allyl trihalosilanes)[11] would likely perturb the energies of the synclinal transition states more profoundly.

The syn diastereomer is often produced in these reactions with high diastereoselectivity. An oft-cited rationale for the observed diastereoselectivity invokes the minimization of steric repulsion by proceeding through antiperiplanar transition states.[6f] The antiperiplanar transition state leading to the anti diastereomer (**anti-1**, Scheme 3) is considered to exhibit more severe gauche interactions between R^1 and R^2 than the corresponding synclinal transition state (**syn-1**, Scheme 3).

Scheme 3

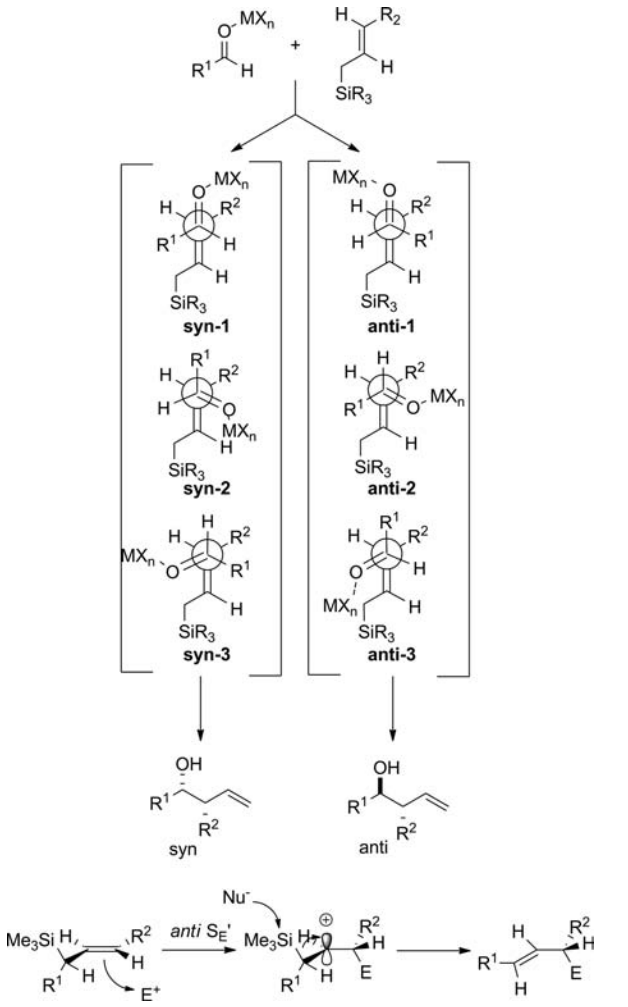

Unfortunately, for intermolecular reactions, it is impossible to determine the precise orientation of the reactants that lead to the observed products. Accordingly, to unambiguously determine the relative orientation of the reactants, a number of models that incorporate both reactants in a single molecule have been devised and examined.

The two most studied models are the subject of a number of detailed investigations from these laboratories (Scheme 4).[12] Model system **A** was designed to probe the preference between transition structures **syn-3** and **anti-1** in the reaction of an *E*-crotylsilane, whereas model system **B** was designed to probe the analogous *Z*-crotylsilane system. The results of these studies revealed that the Lewis acid-promoted reactions afforded predominately the product resulting from a synclinal disposition of double bonds in the transition state. The fluoride-promoted pathway was also investigated, and interestingly, the product resulting from the antiperiplanar transition state is generated in greater amounts. This intriguing divergence in selectivity clearly suggests that multiple factors are operative. Clearly, model systems of this type will be limited in the number of different transition states that can be accessed given the structural constraints of intramolecularity.

2.2. Computational Studies. The allylation of activated carbonyl compounds has also been investigated computationally using quantum mechanical methods.[13−15] An early gas-phase DFT study using BFH_2 as the Lewis acid and

dx.doi.org/10.1021/ja311889v | J. Am. Chem. Soc. 2013, 135, 4743−4756

Scheme 4

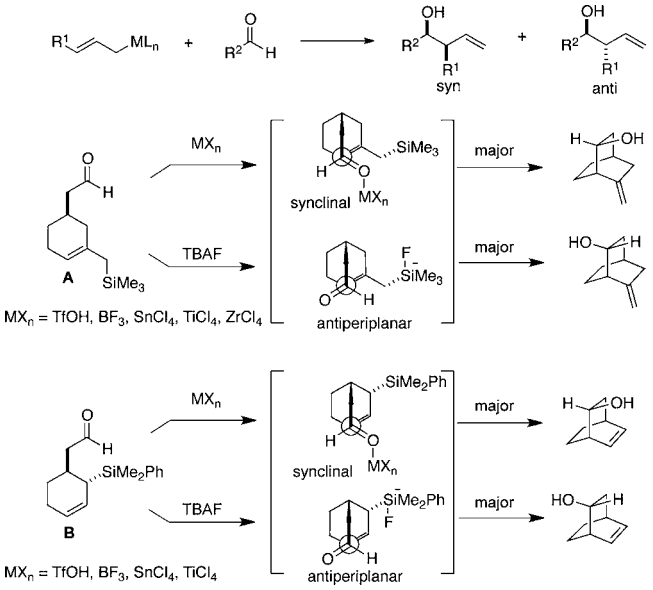

trihydridoallylsilane suggests a pseudocyclic transition state in which the fluorine atom is closely associated with the silicon atom.[14] Intrinsic reaction coordinate (IRC) calculations imply bond formation between the silicon and the fluorine atoms. Only synclinal transition states could be located which is a direct consequence of the proposed Si···F interaction. The model simplifications could have introduced an unjustified bias toward a cyclic transition state which included the use of weaker Lewis acid (BFH_2) and a less hindered, electron-deficient silicon atom than used experimentally. Moreover, the conclusion of such an interaction is invalidated by the experimental demonstration of an anti S_E2' process for allylsilane additions.[12d]

A thorough, combined computational and experimental study on the crotylation of *O*-methyloxocarbenium ions has also been reported.[15] Canonical ensembles of the calculated B3LYP transition states are relatively consistent with the experimentally observed diastereoselectivities that, for the most part, favor the syn diastereomer. Steric repulsion primarily accounts for the formation of the major syn diastereomer. The relative agreement between the predicted and the experimental diastereoselectivities suggests a stepwise process.

2.3. Goals of this Study. The nature and magnitude of the interactions governing the selectivity preferences in open transition structures remain obscure. The deconstruction of the interaction energies in the transition state and/or along the reaction coordinate into physically recognizable quantities, such as steric, electrostatic, orbital, and dispersion should provide additional insights into the stereochemical controlling factors. Such a decomposition process was conceived[16] and implemented[17] by Kitaura and Morokuma a number of years ago. A recently introduced localized orbital method (LMO-EDA)[18] used in this investigation essentially teases out the electrostatic ΔE_{elec}, polarization (intra-orbital mixing) and charge transfer (inter-orbital mixing) ΔE_{pol}, exchange ΔE_{ex}, repulsion ΔE_{rep}, and dispersion ΔE_{disp} (applicable when DFT or post-HF methods are used) energetic contributions from the total interaction energy ΔE_{int} (eq 1).

$$\Delta E_{int} = \Delta E_{elec} + \Delta E_{pol} + \Delta E_{ex} + \Delta E_{rep} + \Delta E_{disp} \quad (1)$$

Although energy decomposition analysis (EDA) methods have been applied to understand weak and strong chemical binding and bonding,[19] the method has seen relatively limited application toward understanding reactivity and selectivity in chemical reactions.[20] Bickelhaupt, Houk, and Ess have pioneered the activation−strain model[20a−d] or synonymously the distortion−interaction model[20e−l] of reactivity to analyze a number of chemical reactions. This method decomposes the energy difference between a point along the reaction coordinate and the minimum from which it originates $\Delta E(\xi)$ (ξ, extent of reaction) to the sum of the interaction energy of the distorted reactants (ΔE_{int}) and the energy required to distort the fragments to that geometry in the absence of any interaction (ΔE_{dist}).

$$\Delta E(\xi) = \Delta E_{int} + \Delta E_{dist} \quad (2)$$

A significant number of reactions have been investigated for which $\Delta E(\xi)$ as a function of structure is more strongly correlated with the distortion energy rather than the energy of interaction ΔE_{int}. This situation will more often be observed for reactions with late transition states and those that have high frequency bending modes along the reaction coordinate.[20e,f] Reactions with earlier transition states are expected to better correlate with the interaction energy component of the total energy which more closely parallels the predictions of FMO theory.

The goal of this study was to reveal which components of the interaction energy contributed most to the observed diastereoselectivity for the addition of (*E*)-2-butenyltrimethylsilane to acetaldehyde under activation by BF_3, hydronium ion, and fluoride ion. The first stage in the program required locating the six staggered transition structures for which DFT was the chosen theoretical approach. Next, the energies for each transition structure were decomposed along their respective reaction coordinates. Then for each reaction, the components of the interaction energy that contributed most to the diastereoselectivity were identified, and the EDA results were validated through assessment of geometrical and electron density properties. The analysis would ideally provide a better understanding of the selectivity controlling factors in the allylation of aldehydes and other open transition-state reactions, such as Mukaiyama-type aldol[21] and Michael[22] addition reactions.

3. COMPUTATIONAL METHODS

All geometries were fully optimized using the M06-2X[23] density functional in conjunction with the 6-31+G(d,p) basis set for all atoms. The CPCM model[24] was used for inclusion of dichloromethane as solvent for all optimizations. The nature of all stationary points was determined by seminumerical (numerical differentiation of analytically computed first derivatives) computation of vibrational frequencies which were used for obtaining zero-point vibrational energies at 195 K, and the "quasiharmonic approximation"[25] (with all frequencies below 80 cm^{-1} being replaced by 80 cm^{-1} for computing free energies) was used for reducing error from the use of the harmonic oscillator approximation for low-frequency normal modes. A scaling factor of 0.967 was used for calculating ZPE.[26] The electronic energies were further refined using the 6-311+G(2d,2p) basis set. Interaction energy decomposition was performed using the LMO-EDA method.[18] Natural population analysis and perturbation theory energy analysis were performed using NBO 3.1 within Gaussian09.[27] All geometry optimizations and LMO-EDA were performed using the GAMESS[28] program.

dx.doi.org/10.1021/ja311889v | J. Am. Chem. Soc. 2013, 135, 4743−4756

4. RESULTS AND DISCUSSION

4.1. Reaction Mechanism. *4.1.1. BF_3-Promoted Addition.* Previous computational studies on the reaction mechanism of BF_3-promoted addition of (*E*)-2-butenyltrimethylsilane to acetaldehyde (Scheme 5) have focused on simplified systems and did not probe the entire transformation from reactants to products. For example, side processes, such as oxetane[29] formation, have not been accounted for, and the desilylation step remains uninvestigated. Moreover, the experimentally documented formation of fluorotrimethylsilane at a temperature of −80 °C needs to be reconciled.[30] More importantly, the potential influence of steps subsequent to carbon−carbon bond formation on the diastereoselectivity has not been considered in detail.

Scheme 5

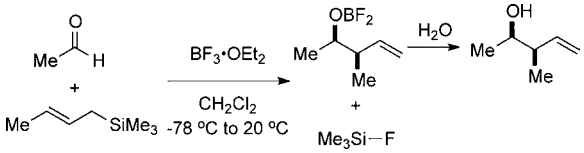

A potential energy diagram was mapped out for the BF_3-promoted crotylation of acetaldehyde (Figure 1) to gain a better understanding of the reaction mechanism, particularly the fate of the intermediate after C−C bond formation. Initial complexation of $BF_3{\cdot}OMe_2$ to acetaldehyde is thermodynamically unfavorable ($\Delta G_{1\rightarrow 2a}$ = 3.3 kcal/mol; $\Delta G_{1\rightarrow 2b}$ = 4.7 kcal/mol), which is consistent with the stronger Lewis basicity of ethers relative to aldehydes[31] and more than compensates for the partial charge delocalization from aldehyde complexation. Formation of the anti isomer **2a** is more favorable than the corresponding syn isomer **2b** ($\Delta\Delta G$ = 1.4 kcal/mol). This well-established thermodynamic preference[32] together with the attendant, enhanced activation of the carbonyl group (evidenced by the greater LUMO lowering (∼0.04 eV) of **2a** compared to **2b**, resulting from more effective complexation), suggests that the reaction is primarily proceeding through anti isomer, **2a**.

Association of the aldehyde-BF_3 complex **2a** with (*E*)-2-butenyltrimethylsilane results in the formation of pretransition-state complex **3**. A transition state connecting **2a** to **3** was not investigated. Similar pretransition-state complexes have been invoked in the structurally similar Mukaiyama aldol reaction in gas-phase computational studies.[33] The physical nature of complex **3** was probed through an EDA of the reactants and can best be described as a charge-transfer/van der Waals complex.[34]

Complex **3** next proceeds through transition state $\mathbf{4}^{\ddagger}$ to form intermediate **5** in a considerably endergonic step ($\Delta G_{3\rightarrow 5}$ = 5.5 kcal/mol) (Figure 1). Intermediate **5** may proceed through at least six readily accessible pathways ($\mathbf{4}^{\ddagger}$, $\mathbf{6}^{\ddagger}$, $\mathbf{7}^{\ddagger}$, $\mathbf{8}^{\ddagger}$, $\mathbf{9}^{\ddagger}$, $\mathbf{11}^{\ddagger}$). Reversion (via $\mathbf{4}^{\ddagger}$) is actually the lowest-energy pathway with a barrier of only $\Delta G^{\ddagger}_{5\rightarrow 4}$ = 1.8 kcal/mol. Desilylation of **5** is

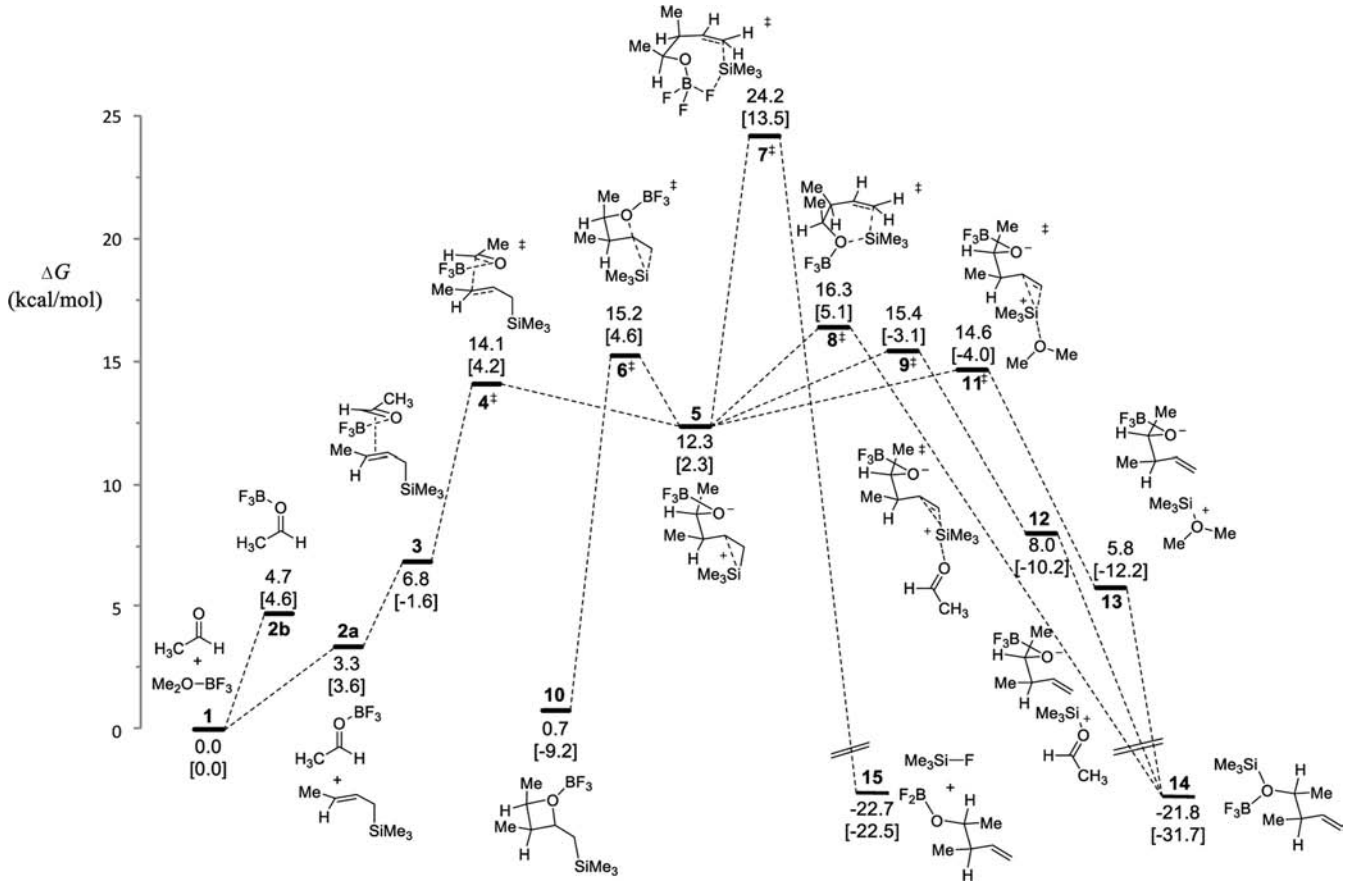

Figure 1. Energy diagram illustrating reaction pathways investigated for the $BF_3{\cdot}OMe_2$-promoted crotylation of acetaldehyde. Relative energy values are represented as free energies *G* (kcal/mol) and are calculated at the CPCM(CH_2Cl_2)-M06-2X/6-311+G(2d,2p)//CPCM(CH_2Cl_2)-M06-2X/6-31+G(d,p) level. Energies in brackets represent enthalpies *H* (kcal/mol). Thermodynamic quantities are determined at 195 K.

dx.doi.org/10.1021/ja311889v | J. Am. Chem. Soc. 2013, 135, 4743−4756

necessary to proceed toward the observed products, and multiple pathways can be envisioned to effect this process. Intramolecular transfer of the silyl group to the fluorine atom with concomitant Si−F cleavage via an eight-membered transition state $7^{‡}$ to generate product **15** and fluorotrimethylsilane directly is the highest-energy pathway ($\Delta G^{‡}_{5\rightarrow 7}$ = 11.9 kcal/mol) and is thus less likely to contribute. This finding is in contrast to previous computational studies suggesting direct fluorine to silicon transfer.[30] Intramolecular transfer of the silyl group to the oxygen atom via a six-membered transition state $8^{‡}$ is a more favorable pathway ($\Delta G^{‡}_{5\rightarrow 8}$ = 4.0 kcal/mol), but there are still accessible lower-energy pathways. Alternatively, external nucleophiles can serve as desilylating agents in bimolecular steps. However, the only stable nucleophiles present in solution are the aldehyde reactant and the dimethyl ether that is decomplexed. Free fluoride ion is unlikely to be present in solution to effect desilylation. Desilylation carried out by dimethyl ether ($\Delta G^{‡}_{5\rightarrow 11}$ = 2.3 kcal/mol) or acetaldehyde ($\Delta G^{‡}_{5\rightarrow 9}$ = 3.1 kcal/mol) provides lower-energy alternatives to the intramolecular transfer via $7^{‡}$ and $8^{‡}$. Acetaldehyde and dimethyl ether serve to shuttle the silyl group to the oxygen via intermediate ion pairs **13** and **12**, respectively, to form highly stable product **14**. Conversion of ion pairs **12** and **13** to product **14** is expected to be near barrierless, and thus transition states were not investigated that lead to **14**.

The formation of fluorotrimethylsilane suggests the need for the conversion of product **14** to product **15**. Deprotection of silyl ethers with BF_3 can be performed experimentally, supporting the conversion of **14** to **15**. Product **15** likely either dimerizes[35] or coordinates with dimethyl ether to increase the thermodynamic preference.[36]

The broad energy landscape accessible to intermediate **5** equates to a complex dependence of the diastereoselectivity on the energies of multiple stationary points, including transition-state energies to C−C bond formation that lead to **5** and the transition-state energies of desilylation. Modeling results with $TiCl_4$ support a less broad energy surface for which the initial barrier primarily dictates the diastereoselectivity.[37] Even though the BF_3-promoted pathway may be complicated by reversibility, the critical, stereodetermining C−C bond forming step was investigated more thoroughly with respect to the topological approach of the activated aldehyde as a model for systems that do not exhibit potential reversibility, such as was found for $TiCl_4$.

4.2. Stereodetermining Transition States. *4.2.1. Geometries and Energies. 4.2.1.1. BF_3-Promoted Pathway.* All six transition-state structures for the BF_3-promoted crotylation of acetaldehyde were located and are provided in Figure 2. The geometries compare reasonably well with those obtained from a recent computational study on the diastereoselectivity in the Mukaiyama aldol reaction.[38] As expected from the difference in nucleophile reactivity, the transition states obtained here are considerably later. For the synclinal conformations, all bonds are arranged with roughly staggered orientations. The anti conformations are perturbed slightly from the idealized 180° dihedral angle for staggered orientations displaying dihedral angles of 187° and 185°. The distances between the carbon atoms undergoing bond formation are very similar (1.97 ± 0.02 Å). The predicted energies reveal a preference for the transition states leading to the syn diastereomer, particularly through transition state **syn-T3-L**[39] that possesses a synclinal arrangement of double bonds. The two antiperiplanar transition states

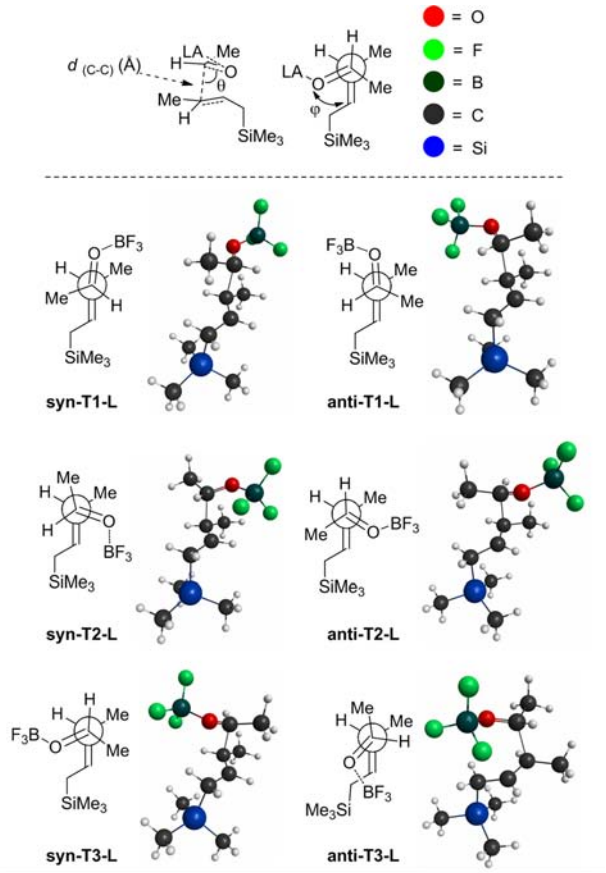

	$\Delta G^{‡}$ [$\Delta H^{‡}$]^a	d^b	θ ^{c}	φ ^{d}
syn-T1-L	4.2 [4.7]	1.99	101.7	187.2
syn-T2-L	0.8 [0.9]	1.96	108.7	273.2
syn-T3-L	0.0 [0.0]	1.95	110.9	66.9
anti-T1-L	2.0 [2.1]	1.96	102.1	184.5
anti-T2-L	3.0 [3.1]	1.96	112.1	296.9
anti-T3-L	1.0 [1.8]	2.00	113.3	42.6

Figure 2. Six transition states for BF_3-promoted crotylation. [a]Relative transition-state energies ($\Delta G^{‡}$ and $\Delta H^{‡}$) in kcal/mol. [b]C(1)−C(2) bond distance (Å). [c]Approach angle (°). [d]Dihedral angle (°).

(**syn-T1-L** and **anti-T1-L**), which are commonly invoked as providing lower-energy channels because of minimized steric interactions,[6f] do not possess the lowest energies of the six structures. These relative energy values suggest that steric interactions may not be important contributors to the overall diastereoselectivity compared to other energetic components.

4.2.1.2. Brønsted Acid Promoted Pathway. The crotylsilane addition through Brønsted acid activation was also investigated. This mode effectively removes any steric influence that the Lewis acid may impart. A single water molecule was used to attenuate its level of activation, as relaxed coordinate scans in the absence of a water molecule suggest a barrierless bond formation. The location of the proton in the activated carbonyl group presents some ambiguity, however its position has little influence on the energies of either the reactants or the transition states.[40] To be geometrically consistent with other Lewis acids, the proton is situated synperiplanar to the aldehydic hydrogen.[41]

Some of the transition states deviate from idealized staggered conformations (Figure 3). Antiperiplanar transition state **syn-**

dx.doi.org/10.1021/ja311889v | J. Am. Chem. Soc. 2013, 135, 4743−4756

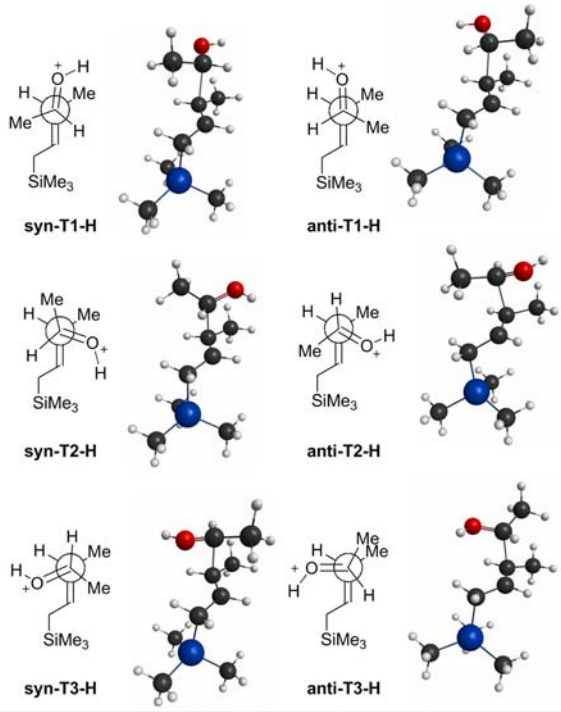

	$\Delta G^{\ddagger}$ [$\Delta H^{\ddagger}$]	d	θ	φ
syn-T1-H	3.0 [3.0]	2.16	98.4	189.9
syn-T2-H	1.7 [1.6]	2.08	104.9	256.0
syn-T3-H	0.0 [0.0]	2.24	106.9	76.9
anti-T1-H	2.8 [2.2]	2.13	98.7	175.8
anti-T2-H	1.8 [1.6]	2.16	107.5	281.9
anti-T3-H	3.1 [2.6]	2.13	103.1	92.8

Figure 3. Six transition states for Brønsted acid-promoted crotylation. Water is excluded for clarity. See Figure 2 for legend.

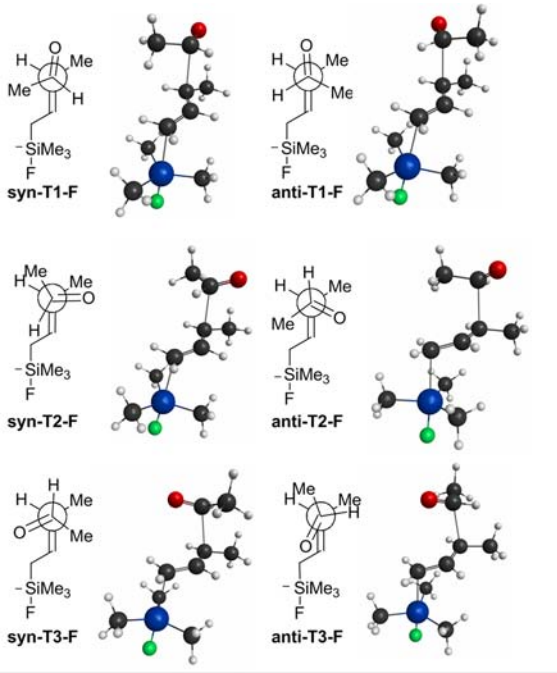

	$\Delta G^{\ddagger}$ [$\Delta H^{\ddagger}$]	d	θ	φ
syn-T1-F	1.1 [0.9]	2.30	105.6	206.1
syn-T2-F	2.4 [2.3]	2.28	108.6	265.6
syn-T3-F	1.4 [1.4]	2.22	109.4	68.5
anti-T1-F	0.0 [0.0]	2.23	105.0	175.0
anti-T2-F	2.5 [2.3]	2.22	110.2	284.9
anti-T3-F	4.0 [3.7]	2.30	113.2	27.5

Figure 4. Six transition states for fluoride-promoted crotylation. See Figure 2 for legend.

T1-H adopts a 190° dihedral angle, likely in an effort to relieve unfavorable interaction between the methyl group of the aldehyde and the TMS-CH_2 group. Whereas all the synclinal transition states for the BF_3-mediated allylation exhibit a smaller dihedral angle in which the oxygen atom is positioned close to the partially positively charged carbon atom of the crotylsilane, all of the synclinal conformations for the proton-mediated pathway deviate from this orientation by maximizing the distance between the protonated oxygen and the carbon atom C(1) gaining the positive charge. This preference likely results from electrostatic repulsion considering the fact that transition state **anti-T3-H** positions the two methyl groups in a near eclipsed conformation to provide sufficient distance between the partially positively charged atoms. The electrostatic gain in energy by avoiding repulsion more than compensates for the loss in energy from unfavorable steric interactions.

4.2.1.3. Fluoride-Promoted Pathway. The fluoride-promoted pathway illustrates interesting contrasts with the BF_3 and Brønsted acid-promoted pathways (Figure 4). Both antiperiplanar transition states are lower in energy than all four synclinal transition states, in contradistinction to the Lewis acid-containing transition states. As was seen in the Lewis acid-promoted reactions, **anti-T1-F** is the lower energy of the two antiperiplanar transition states. Generally the dihedral angles more closely resemble those of the BF_3-bound transition states. Structure **syn-T3-F** is the lowest-energy synclinal transition state as was also observed for both Lewis acid-bound transition states.

To summarize this section, the activation energies reveal that the electrophilically activated pathways show a preference for the formation of the syn diastereomer specifically through the **syn-T3** transition state. The formation of the competing anti diastereomer takes place via **anti-T2-L** and **anti-T1-H**. In comparison, the nucleophilically activated pathway exhibits a preference for formation of the anti diastereomer via the antiperiplanar **anti-T1-F** transition state. These results are in accordance with experimental findings.[6k] The factors that influence the reactivity differences in each pathway as well as the divergence in diastereoselectivity between the electrophilically and nucleophilically activated pathways will be addressed using EDA in the following sections.

4.2.2. EDA of Transition States. The interaction energies between the aldehyde and allylsilane partners for all transition states were decomposed to reveal the relative contributions of the individual components of the interaction energy as well as the distortion energy to the total energy $\Delta E^{\ddagger}$. For completeness, the energies of distortion of each reactant are also included in the analysis. With the inclusion of reactant distortion energies, the total electronic activation barrier $\Delta E^{\ddagger}$ can be expressed as $\Delta E^{\ddagger} = \Delta E_{int}{}^{\ddagger} + \Delta E_d{}^{\ddagger}(A) + \Delta E_d{}^{\ddagger}(B)$.[42] The variation in solvation energies ($E_{solv}{}^{\ddagger} - E_{gas}{}^{\ddagger}$) is not included in this decomposition but is nevertheless small and does not explain the variation in the transition-state energies.[43]

dx.doi.org/10.1021/ja311889v | J. Am. Chem. Soc. 2013, 135, 4743−4756

Table 1. Energy Decomposition Analysis of Reactants in Transition States for All Three Modes of Activation[a]

TS	$\Delta E_{es}^{\ddagger}$	$\Delta E_{exrep}^{\ddagger}$	$\Delta E_{pol}^{\ddagger}$	$\Delta E_{disp}^{\ddagger}$	$\Delta E_{d}^{\ddagger}$(A)[b]	$\Delta E_{d}^{\ddagger}$(B)[c]	$\Delta E_{int}^{\ddagger}$	$\Delta E^{\ddagger}$[d]
syn-T1-L[e]	−34.2	120.5	−84.6	−29.6	21.8	10.2	−27.9	4.1
syn-T2-L	−44.5	143.7	−98.2	−33.2	24.0	8.0	−32.2	−0.2
syn-T3-L	−42.0	137.8	−96.5	−30.8	23.1	7.5	−31.5	−0.9
anti-T1-L	−38.6	128.3	−90.1	−28.7	22.4	7.8	−29.1	1.1
anti-T2-L	−42.9	139.7	−96	−31.3	23.9	9.1	−30.5	2.4
anti-T3-L	−33.3	122.9	−86.4	−31.3	21.4	8.3	−28.1	1.6
syn-T1-H[f]	11.5	84	−91.9	−25.0	14.0	5.5	−21.4	−1.9
syn-T2-H	−4.21	120.1	−117.7	−27.7	21.5	4.0	−29.5	−4.0
syn-T3-H	15.5	77.2	−86.4	−24.0	10.3	2.3	−17.7	−5.0
anti-T1-H	9.7	89.9	−96.7	−24.9	14.3	4.1	−22.0	−3.6
anti-T2-H	7.2	94.5	−97.6	−26.9	14.7	4.3	−22.7	−3.7
anti-T3-H	0.9	107.0	−106.7	−28.0	19.0	4.8	−26.8	−3.0
syn-T1-F[g]	5.8	74.8	−71.7	−20.5	6.5	10.0	−11.6	4.9
syn-T2-F	4.9	78.3	−74.2	−19.9	7.2	9.9	−10.9	6.2
syn-T3-F	7.9	83.9	−81.3	−21.7	7.5	9.0	−11.2	5.2
anti-T1-F	3.6	80.3	−74.6	−21.6	7.2	9.0	−12.2	4.0
anti-T2-F	2.1	86.9	−78.3	−21.4	7.9	9.4	−10.7	6.6
anti-T3-F	13.5	72.8	−76.7	−19.5	6.8	10.4	−9.9	7.2

[a]All energies are in units of kcal/mol. [b]Distortion energy of aldehyde component. [c]Distortion energy of crotylsilane component. [d]$\Delta E^{\ddagger} = \Delta E_{d}^{\ddagger}(A) + \Delta E_{d}^{\ddagger}(B) + \Delta E_{int}^{\ddagger}$ [e]BF_3-promoted pathway [f]Brønsted acid-promoted pathway [g]Fluoride-promoted pathway.

The transition states for the BF_3-promoted reaction are the latest along the reaction coordinate as well as being the most endergonic, hence a greater degree of distortion is necessary to achieve suitable levels of interaction as is observed (Table 1). The lowest-energy transition state **syn-T3-L** does possess the second highest interaction energy behind **syn-T2-L** as well as the lowest energy of distortion of the crotylsilane component ΔE_d(B). Transition state **anti-T1-L**, however, has the next lowest energy required to distort the crotylsilane component ΔE_d(B). The antiperiplanar transition states **syn-T1-L** and **anti-T1-L** have the lowest steric contribution $\Delta E_{exrep}^{\ddagger}$, which is the traditional rationale for its status as the preferred transition state.[6f] Although **syn-T1-L** is sterically the most preferred transition state, it suffers from a relatively low preference in terms of orbital $\Delta E_{pol}^{\ddagger}$ and electrostatic interactions $\Delta E_{es}^{\ddagger}$. Overall, the energetic preference for transition state **syn-T3-L** can be attributed to a combination of favorable electrostatic and orbital interactions and a low energy of distortion of the allylsilane component.

The energy breakdown in the Brønsted acid-mediated pathway is similar to the BF_3-mediated pathway. A marked distinction is the earlier nature of the lowest-energy transition state **syn-3-H** (d = 2.24 Å). Counterintuitively, **syn-T3-H** also possesses the most unfavorable interaction energy. For every component of the interaction energy, excluding a substantially favorable steric component ($\Delta E_{exrep}^{\ddagger}$), **syn-T3-H** exhibits the weakest interaction. The smaller favorable energies in **syn-T3-H** are compensated for by highly favorable distortion energies for both the aldehyde and allylsilane components.

The fluoride-promoted pathway generally has high reaction barriers, but the reaction is concerted, after pre-equilibrium formation of a pentacoordinated fluorosilicate. The lowest-energy transition states are antiperiplanar (**syn-T1-F** and **anti-T1-F**) with **anti-T1-F** being slightly lower (0.9 kcal/mol). Analysis of the energetic contributions of this pathway is complex because all components of the interaction energy influence $\Delta E^{\ddagger}$ to a similar extent. However, the antiperiplanar transition states do appear to benefit from decreased steric ($\Delta E_{exrep}^{\ddagger}$) and favorable electrostatic ($\Delta E_{es}^{\ddagger}$) interactions, whereas the synclinal transition states **syn-T3-F** and **anti-T2-F** exhibit the strongest orbital interactions ($\Delta E_{pol}^{\ddagger}$). The electrostatic preference for antiperiplanar TS's contrasts the electrophilically activated pathways in which the synclinal transition states are electrostatically preferred. The role of distortion energy is not as significant in the fluoride-promoted pathway.

In summary, for the BF_3-promoted pathway, the antiperiplanar transition states are preferred sterically, whereas the synclinal transition states are preferred through electrostatic and orbital interactions. The combination of these factors renders **syn-T3-L** the energetically preferred transition state overall. The Brønsted acid-promoted pathway is complicated by significant variation in distortion energy. For the fluoride-promoted pathway antiperiplanar transition states are preferred overall because of favorable steric and electrostatic (contrary to the BF_3-promoted pathway) interactions while favoring the synclinal transition states through orbital interactions.

4.2.2.1. Rationalization of Diastereoselectivity. To a first approximation, the overall diastereoselectivity can be rationalized by the difference between the lowest-energy transition state leading the syn diastereomer and the lowest-energy transition state leading to the anti diastereomer (Table 1). Each bar in the graphs in Figure 5 represents the difference for the indicated component of the overall energy ($\Delta E^{\ddagger}$) between the lowest-energy syn transition state versus the lowest-energy anti transition state ($\Delta\Delta E_x < 0$ reflects a preference for the syn transition state for energy component x, while $\Delta\Delta E_x > 0$ reflects an anti preference).

The transition states for the BF_3-promoted process exhibit a small difference in distortion energy ($\Delta E_{d}^{\ddagger}$) reflecting similar extents of bond formation at the transition state. Although sterically unfavorable, transition state **syn-T3-L** benefits from considerably favorable electrostatic and orbital interactions. The diastereoselectivity for the BF_3-promoted process is thus

dx.doi.org/10.1021/ja311889v | J. Am. Chem. Soc. 2013, 135, 4743−4756

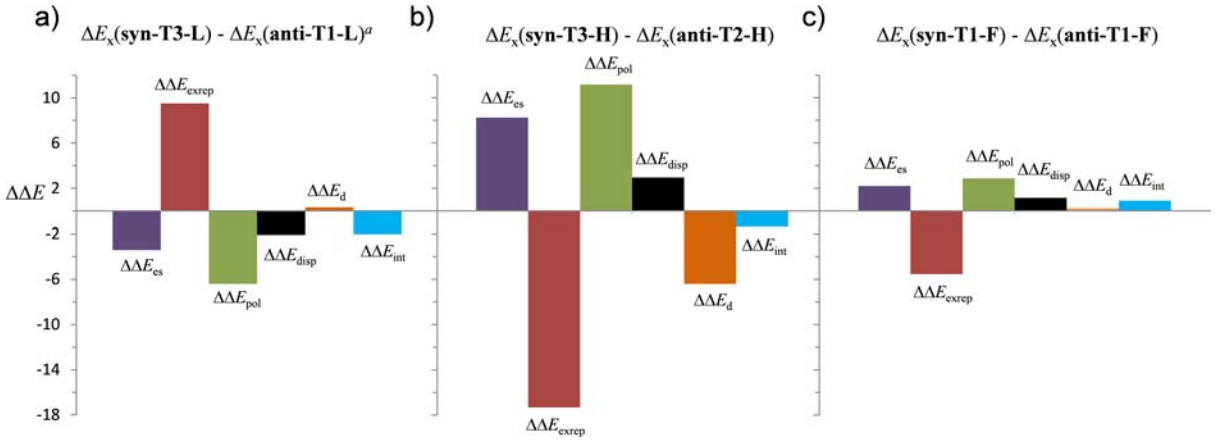

Figure 5. Differences in components of interaction energy between two lowest-energy different transition states in each activation mode in kcal/mol: (a) BF_3, (b) H^+, (c) F^-. [a] x = es, exrep, pol, disp, d, int.

largely attributed to favorable electrostatic ΔE_{es} and orbital ΔE_{pol} terms for **syn-T3-L**.

For the Brønsted acid-promoted pathway, the lowest-energy transition state is particularly early ($d_{C(1)-C(2)}$ = 2.24 Å) compared to all other transition states for this pathway (Figure 3). The early nature is reflected in a smaller ΔE_d. The low energy of distortion and steric interactions for **syn-T3-H** accounts for the diastereoselectivity observed in the Brønsted acid-promoted pathway. The origin of the favorable distortion level for **syn-T3-H** is the subject of a forthcoming section.

The diastereoselectivity in the fluoride-promoted reaction is largely accounted for by the difference in the energies of the antiperiplanar transition states. The greatest energetic contributor to the transition-state energy difference is steric interactions (ΔE_{exrep}) in preference for transition state **syn-T1-F**. However the combination of favorable electrostatic (ΔE_{es}), orbital (ΔE_{pol}), and dispersion (ΔE_{disp}) terms results in the overall energetic preference for **anti-T1-F**.

The variation in distortion has a significant impact on the energies of competing transition-state conformations and consequentially the diastereoselectivity. Decomposition of the interaction energy alone is not sufficient for a complete understanding of this variation. Uncovering the origin of the variation in the distortion energies would provide a more complete rationalization of the observed diastereoselectivities and is the focus of the following sections.

4.3. Origin of Variation in Distortion. The origins of the variation in distortion can be better understood if that variation can be explained by components of the interaction energy. This analysis can potentially be achieved by comparison of ΔE_{int} at constant distortion ($\Delta E_{int,d}$) among multiple transition states and may be considered viable when a linear relationship exists between $\Delta E_{int,d}$ and $\Delta E^{\ddagger}$. This procedure allows the investigation of the components of the interaction energy close to the transition state that best account for the variation in $\Delta E_d(\xi)$.

The transfer in variation was achieved by performing an EDA on selected points along the reaction coordinate for all transition states. Each component of the energy was plotted as a function of $\Delta E_d(\xi)$ and fitted to a parabolic curve. The energies were interpolated on the basis of a parabolic fit.[44] The optimal $\Delta E_d(\xi)$ was chosen based on the correlation between $\Delta E^{\ddagger}$ and $\Delta E_{int,d}(\xi) + \Delta E_d(\xi)$ for all of the pathways.[45]

A linear relationship is expected between $\Delta E^{\ddagger}$ and $\Delta E_{int,d}(\xi) + \Delta E_d(\xi)$ if the change in energy from distortion at small variations in ξ near the transition state is approximately equal to the energy gained by interaction ($dE_{int}/d\xi \approx -dE_d/d\xi$) for all transition states (low curvature at the transition state). All three pathways exhibit $\Delta E_d(\xi)$ values in the range of the distortion levels at the transition states $\Delta E_d^{\ddagger}$ for their respective reactions. Strong linear trends are observed and thus validate the comparison of the components of the interaction energy (ΔE_{int}) at the corresponding constant levels of distortion.[46]

The distortion energy difference in Figure 5 for the BF_3 and fluoride-promoted pathways is small, and thus its distribution among the different interaction energies results in only small differences from Figure 5. This is not the case within other transition-state comparisons and will be addressed in a later section.

The difference in distortion for the Brønsted acid-mediated pathway, however, between the synclinal transition-state pathways **syn-T3-H** and **anti-T2-H** is significant at a value of 6.4 kcal/mol (Table 1 and Figure 5), favoring the **syn-T3-H** pathway. This large difference in distortion leads to a very different interaction energy landscape at constant distortion than at the distortion level of the transition state (compare difference in Table 1 vs Table 2).[47] Whereas, the only energy components that favor **syn-T3-H** at the transition state are ΔE_{exrep} and ΔE_d (6.4 kcal/mol, Figure 5), all of the energy components favor **syn-T3-H** at constant distortion except for ΔE_{exrep} and ΔE_{disp}. Thus, the origin of the large distortion energy difference favoring **syn-T3-H** at the transition state is accounted for mostly by a large favorable orbital term ΔE_{pol}.

Table 2. Energetic Components at Constant Levels of Distortion[a]

TS	$\Delta E_{es,d}^{\ddagger}$	$\Delta E_{exrep,d}^{\ddagger}$	$\Delta E_{pol,d}^{\ddagger}$	$\Delta E_{disp,d}^{\ddagger}$	$\Delta E_{int,d}^{\ddagger}$
syn-T1-H	13.5	79.4	−87.9	−24.6	−19.6
syn-T2-H	7.0	94.7	−97.8	−25.9	−21.9
syn-T3-H	8.0	94.2	−99.3	−25.6	−22.7
anti-T1-H	10.6	87.9	−95.0	−24.8	−21.3
anti-T2-H	8.9	90.9	−94.5	−26.6	−21.4
anti-T3-H	9.7	87.6	−91.7	−26.4	−20.8

[a]Values for Brønsted acid pathway are interpolated at $\Delta E_d(\xi)$ = 17.7 kcal/mol.

dx.doi.org/10.1021/ja311889v | J. Am. Chem. Soc. 2013, 135, 4743−4756

Table 3. Orbital Energy Differences (Δ_x[a] and $\Delta_x^{\ddagger}$[b]) and Charge Transfer (Δq_x[c])

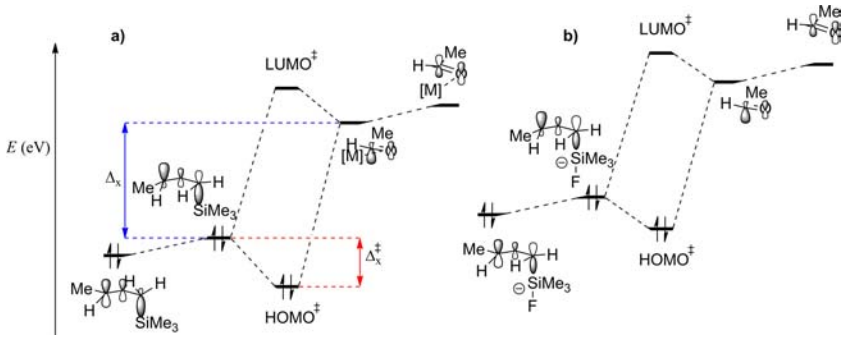

	syn-T1	syn-T2	syn-T3	anti-T1	anti-T2	anti-T3
$\Delta_L^{\ddagger}$	1.39	1.50	1.60	1.54	1.47	1.50
Δ_L	4.18	4.18	4.07	4.07	4.18	4.19
Δq_L	0.473	0.528	0.541	0.522	0.526	0.525
$\Delta_H^{\ddagger}$	1.59	1.72	1.75	1.67	1.66	1.63
Δ_H	4.08	4.00	4.02	4.02	4.08	4.08
Δq_H	0.363	0.395	0.406	0.389	0.393	0.373
$\Delta_F^{\ddagger}$	0.64	0.60	0.69	0.71	0.53	0.64
Δ_F	3.81	3.81	3.85	3.79	3.98	3.80
Δq_F	0.316	0.315	0.330	0.318	0.326	0.293

[a]Frontier orbital energy difference of distorted reactants (eV). [b]Difference in energy between HOMO of the distorted reactant and the HOMO of the transition state (eV). [c]Charge transfer determined from NBO charges.

The origin of the enhanced orbital interactions favoring **syn-T3** for all activation manifolds remains unclear at this point.[48] A frontier orbital energy analysis can be used to dissect the orbital interactions into contributions from orbital overlap and frontier orbital energy differences in the reacting components, which is the focus of the following sections.

4.4. Orbital Energy Analysis. *4.4.1. Rationalizing Synclinal Selectivity.* The foregoing analysis revealed that in the electrophilic activation manifolds, the preference for **syn-T3-L** and **syn-3T-H** pathways is attributed to increased orbital interactions and to a lesser extent, electrostatic interactions and that in the nucleophilic activation manifold, the preference for antiperiplanar **anti-T1-F** is attributed to decreased steric and electrostatic repulsion. Nevertheless, the most favorable transition state leading to a syn product, **syn-T3-F**, possesses the greatest orbital interactions. The nature of this increased orbital interaction term for those synclinal transition states is next examined by a frontier orbital energy analysis.

The figure (a) in Table 3 depicts the orbital energy diagram for the BF_3-promoted and Brønsted acid-promoted pathways and figure (b) depicts the fluoride-promoted pathway. The HOMO for the undistorted crotylsilane is shown on the far left and the LUMO of the undistorted aldehyde component is shown on the far right in both figures. The nuclei are then allowed to distort to the transition-state geometries and the energies of the resulting distorted orbitals are then determined. The resulting distorted orbitals are allowed to mix causing the orbital splitting in the transition states which is shown in the center of the diagrams, corresponding to HOMO‡ and LUMO‡.

Under second-order perturbation theory,[49] the amount that the HOMO‡ energy is lowered relative to the HOMO of the crotylsilane component ($\Delta_x^{\ddagger}$) is dependent on both the HOMO−LUMO gap (Δ_x) of the reactants, the resonance energy associated with the overlap region, and the exchange-corrected Coulombic repulsion contributions. The amount of charge transfer (Δq_x) in the transition state from the crotylsilane to the activated aldehyde component is listed in Table 3.[50] The charge transfer includes effects from both resonance energy from orbital overlap and Δ_x.

In comparing synclinal transition state **syn-T3-L** to antiperiplanar transition state **anti-T1-L**, the orbital energy differences Δ_L are equivalent (Δ_L(**syn-T3**) = Δ_L(**anti-T1**), Table 3). This equivalence means that the distortion of the reactants leads to equivalent frontier orbital energy separation. However, the charge transfer is greater for **syn-T3-L** (Δq_L = 0.541) than for **anti-T1-L** (Δq_L = 0.522). This greater charge transfer is confluent with the lowering of the HOMO‡ for **syn-T3-L** ($\Delta_L^{\ddagger}$ = 1.60 eV) compared to **anti-T1-L** ($\Delta_L^{\ddagger}$ = 1.54 eV). Thus, the preference for the **syn-T3-L** transition state arises from greater charge transfer, which is in turn due to greater orbital overlap rather than a narrowing of the frontier orbital energy gap of the distorted reactants.[51] Similar conclusions can be drawn from the Brønsted acid-mediated pathway.

Under fluoride activation, the energetically preferred pathways are both antiperiplanar, **syn-T1-F** and **anti-T1-F** with a slight preference for **anti-T1-F** ($\Delta\Delta E^{\ddagger}$ = 0.9 kcal/mol, Table 1). Pathway **anti-T1-F** has a slightly smaller Δ_F ($\Delta\Delta_F$ = −0.02 eV), negligible charge transfer Δq_F ($\Delta\Delta q_F$ = 0.002 *e*), and a larger $\Delta_F^{\ddagger}$ ($\Delta\Delta_F^{\ddagger}$ = 0.07 eV), which all contribute to an overall preference for **anti-T1-F**. Although **syn-T3-F** is less favorable than both antiperiplanar transition states, it still has the greatest overall charge transfer (Δq_F = 0.330 *e*), illustrating its superior overlap energy. Thus, the primary contributors to the diastereoselectivity in the fluoride-promoted pathway are the steric and electrostatic repulsions that disfavor all four synclinal transition states and the enhanced orbital interactions in **anti-**

dx.doi.org/10.1021/ja311889v | J. Am. Chem. Soc. 2013, 135, 4743−4756

T1-F compared to **syn-T1-F** that favor formation of the anti diastereomer.

Although enhanced orbital interactions accompany all three (−)-synclinal pathways (**syn-T3**), the reasons for this preferred arrangement are not certain. Two possible contributors can be identified: (i) greater intrinsic overlap in the primary interacting orbitals or (ii) in-phase overlap of orbitals not engaged in primary interaction (secondary orbital overlap). In fact, as early as 1986, Ahn and Thanh suggested that secondary orbital overlap could be responsible for the preferred synclinal arrangement of double bonds in the aldol addition reaction.[52] In the following section, the importance of this contribution is investigated.

4.4.2. Do Secondary Orbital Interactions Contribute to the Preference for syn-T3? Secondary orbital interactions (SOIs) are characterized by in-phase orbital overlap between atoms not directly involved in bonding in the HOMO of the transition state. The HOMO of the **syn-3T** transition states for each reaction type qualitatively suggests a region of in-phase overlap between the oxygen atom of the aldehyde and the methylene group of the crotylsilane (Figure 6). If this overlap is sufficiently energetically stabilizing, one might expect enhanced charge transfer and/or a larger $\Delta_L^{\ddagger}$ compared to transition states that do not possess this interaction.

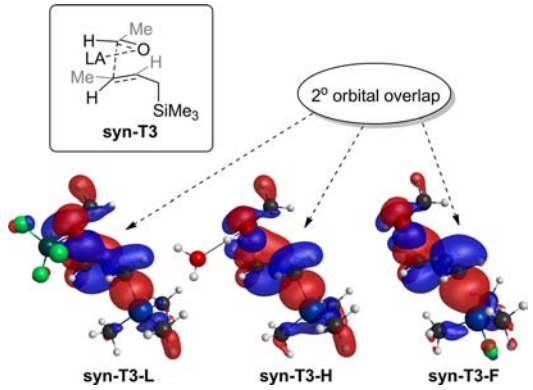

Figure 6. HOMO of transition states (HOMO‡) for **syn-3T-L**, **syn-3T-H**, and **syn-3T-F** with isodensity = 0.03 au.

The approximate contribution from SOIs can be teased out by making relevant transition-state comparisons as illustrated in Figure 7. The quantities that may gauge SOI contributions and their determinations are shown at the bottom of Figure 7 (Δq^{SOI}, $\Delta^{\ddagger,SOI}$, $\Delta E_{pol}{}^{SOI}$, and $\Delta E_{int}{}^{SOI}$).[53] The difference in energy between **syn-T3** and **anti-T2** could furnish the contribution from SOIs because they are both synclinal transition states and the former contains overlap between the aldehyde oxygen and the silylmethylene, whereas the latter does not. However, they also experience different contributions to the four parameters alluded to above because of different steric interactions. These different contributions are: (a) the gauche relationship of the methyl groups in **syn-T3**; (b) the gauche relationship of the methyl group and the Lewis acid in **anti-T2**; and (c) the steric interaction between the methyl and the silylmethylene groups in **anti-T2.** To adumbrate the existence of SOIs, the contributions that these parameters make can be factored out by subtracting the contributions that they make to **anti-T1** from the contributions they make to **syn-T3** to account for interaction (a) above and by subtracting the contributions

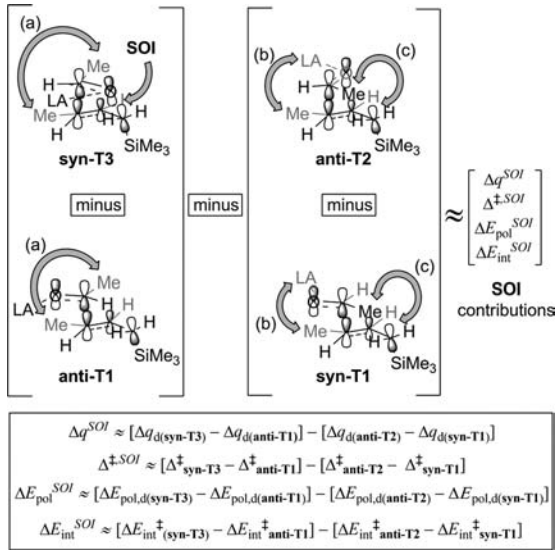

Figure 7. Scheme for determining the contribution from SOIs.

that they make to **syn-T1** from the contributions they make to **anti-T2** to account for interactions (b) and (c) above.[54]

The comparison of the **syn-T3** and **anti-T2** transition states for the BF_3 pathway provides the following results: $\Delta q_L{}^{SOI} = -0.034\ e$, $\Delta_L{}^{\ddagger,SOI} = -0.02$ eV, $\Delta E_{pol}{}^{SOI} = 3.7$ kcal/mol, $\Delta E_{int}{}^{SOI} = -0.4$ kcal/mol. All of these descriptors except $\Delta E_{int}{}^{SOI}$ indicate that SOIs do not make a stabilizing contribution to transition state **syn-T3**.[55] Similar data are obtained from the Brønsted acid-promoted manifold; $\Delta q_H{}^{SOI} = -0.013\ e$, $\Delta_H{}^{\ddagger,SOI} = 0.01$ eV, $\Delta E_{pol}{}^{SOI} = 2.3$ kcal/mol, $\Delta E_{int}{}^{SOI} = 0.4$ kcal/mol. From these results, it can be concluded that SOIs do not contribute significantly to the synclinal preference for **syn-T3**.

The elimination of SOIs as a significant contributor to the diastereoselectivity suggests that the preference can be attributed to enhanced, primary orbital interactions. To identify the contribution of primary orbital interactions, inspection of the transition-state geometries provides valuable insights. For example, differences in geometrical coordinates between two transition states may reveal how achieving optimal primary orbital interactions (as reflected in the near equality of the orbital interaction energies ($\Delta\Delta E_{pol}{}^{\ddagger}_{(anti\text{-}T2\text{-}L\ -\ syn\text{-}T3\text{-}L)} = 0.5$ kcal/mol)) requires different levels of distortion. Inspection of the crotylsilane fragment in the transition state reveals that an additional amount of distortion is present in **anti-T2-L** that is absent in **syn-T3-L** ($\Delta\Delta E_d{}^{\ddagger}_{(anti\text{-}T2\text{-}L\ -\ syn\text{-}T3\text{-}L)} = 1.6$ kcal/mol), namely the distortion of the π-system (Figure 8).[56] This distortion in the crotylsilane is necessary so that the aldehyde can adopt an appropriate approach trajectory in **anti-T2-L** for ideal overlap. The distortion is induced by the steric interaction between the methyl group of the aldehyde and the silylmethylene group. This observation explains why the orbital interactions at a constant level of distortion favor **syn-T3-L** more significantly ($\Delta\Delta E_{pol,d}{}^{\ddagger}_{(anti\text{-}T2\text{-}L-syn\text{-}T3\text{-}L)} = 6.2$ kcal/mol). These conclusions are also consistent with the results from model systems investigated experimentally (Scheme 4).[8c]

In summary, the overall transition-state energy for **syn-T3-L** is lower than **anti-T2-L** because a lesser degree of distortion is required in **syn-T3-L** to achieve the same level of primary orbital overlap compared to **anti-T2-L**. Similar conclusions are reached upon comparing Brønsted acid-mediated transition states (**syn-T3-H** and **anti-T2-H**).

dx.doi.org/10.1021/ja311889v | *J. Am. Chem. Soc.* 2013, 135, 4743−4756

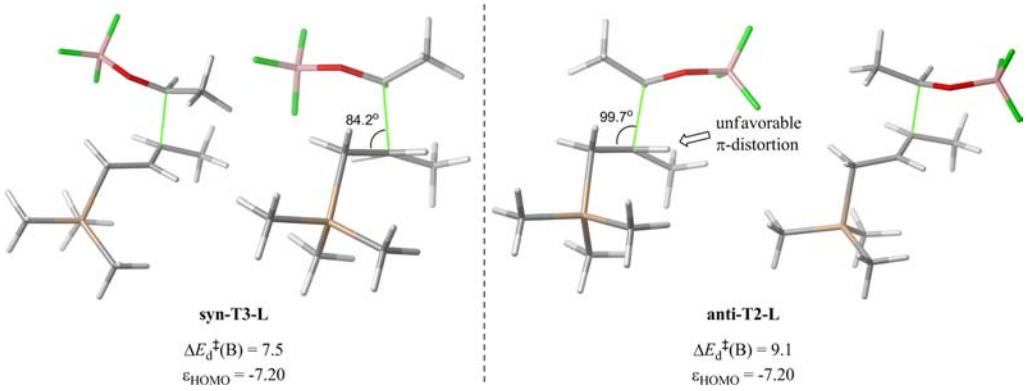

Figure 8. Transition states for **syn-T3-L** and **anti-T2-L** from two perspectives including that from the internuclear axis of the C−C bond of the alkene from the silylmethylene-bound carbon.

4.4.3. What Orbital Interactions Favor Synclinal Over Antiperiplanar? The origin of the enhanced orbital interactions present in synclinal transition state **syn-T3** compared to **anti-T1** or **anti-T2** compared to **syn-T1** has not been elucidated up to this point. The elimination of the SOI involving an in-phase interaction between the oxygen of the aldehyde and the silylmethylene carbon was ruled out because of an insignificant energetic contribution.

A reasonable alternative for the enhanced orbital overlap could be differential primary $\pi\rightarrow\pi^*$ interactions. The differences in the orbital overlap of the FMO's can be seen qualitatively from Figure 9. The distorted FMO's for **syn-T3-L** and **anti-T1-L** as well as the corresponding transition-state HOMO's are shown. The HOMO's of the crotylsilane are very similar for both **syn-T3-L** and **anti-T1-L**. The major difference is the approach of the aldehyde. The portion of the LUMO localized on the carbon of the aldehyde in **syn-T3-L** is directed more inward, toward the alkene π-system, due to the tilted approach, than the portion of the LUMO localized on the carbon of the aldehyde in **anti-T1-L**. The requirement for a Burgi−Dunitz approach angle[57] prevents additional overlap of the aldehyde carbon with the internal alkene carbon in antiperiplanar transition states. The difference in overlap is also borne out by inspection of the transition-state HOMO's. The overlap between the aldehyde carbon and the alkene π-system of the crotylsilane is more centered, while that for **anti-T1-L** is more off-centered which may be expected to translate to decreased overlap energy for **anti-T1-L**.

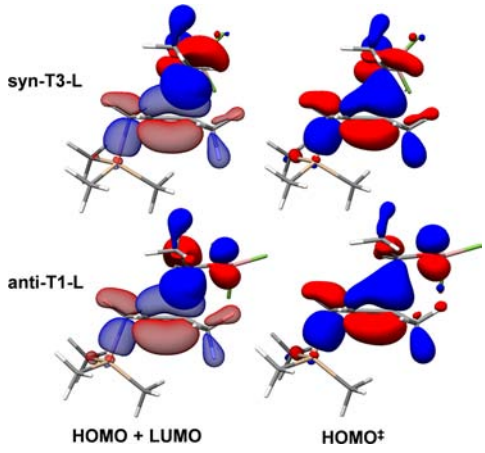

Figure 9. Distorted HOMO of crotylsilane, LUMO of crotylsilane, and transition-state HOMO for **syn-T3-L** and **anti-T1-L**. The HOMO's and LUMO's have values of isodensity = 0.06, while the transition-state HOMO's have an isodensity = 0.05.

The $\pi\rightarrow\pi^*$ interaction of interest was quantified, using second-order perturbation theory through an NBO analysis, at earlier points along the reaction coordinate for each pathway (**syn-T3-L** and **anti-T1-L**), where extensive orbital polarization and mixing has not yet taken place, to approximate the $\pi\rightarrow\pi^*$ interaction difference in the vicinity of the transition state (Figure 10). Figure 10(a) is a plot of the energy difference ($\Delta\Delta E_{\pi\rightarrow\pi^*}$) between the $\pi\rightarrow\pi^*$ interaction for **syn-T3-L** and **anti-T1-L**, respectively. The energy difference increases to $\Delta\Delta E_{\pi\rightarrow\pi^*}$ = 5.3 kcal/mol as the distance approaches d_{c-c} = 2.28 Å. The energy difference also favors **syn-T3-L** upon comparison as a function of distortion (Figure 10(b)). The energy difference $\Delta\Delta E_{\pi\rightarrow\pi^*}$ is approximated to be 6.0 kcal/mol, favoring **syn-T3-L**, at a distortion level of ΔE_d = 11.0 kcal/mol based on linear fits of the two curves (Figure 10(b)). Thus, as a function of both distance and distortion, the **syn-T3-L** pathway exhibits a greater $\pi\rightarrow\pi^*$ interaction energy than the **anti-T1-L** pathway. Similar conclusions can be drawn when comparing synclinal **anti-T2-L** to antiperiplanar **syn-T1-L**. Additionally, bond order results support the importance of enhanced overlap with the internal alkene carbon atom for **syn-T3-L**.[58]

In conclusion, the enhanced orbital interactions in synclinal versus antiperiplanar transition states can be attributed to increased $\pi\rightarrow\pi^*$ interactions. The greater overlap can be explained by the tilted trajectory of the aldehyde in synclinal transition states which directs the aldehyde LUMO toward the center of the π system of the crotylsilane. Moreover, the necessary Burgi−Dunitz approach trajectory[57] prevents the aldehyde in antiperiplanar transition states to engage in additional overlap with the internal alkene carbon atom resulting in diminished overall orbital overlap relative to synclinal transition states.

5. SUMMARY AND CONCLUSIONS

In this study, the origin of diastereoselectivity in the crotylation of acetaldehyde has been examined by computational methods. Under electrophilic activation (BF_3 and Brønsted acid), the syn diastereomer is obtained experimentally with high selectivity, and that selectivity is reproduced in these calculations. In particular, the preferred pathway proceeds via (−)-synclinal transition state **syn-T3** for both activation modes. Under nucleophilic activation (fluoride), the anti diastereomer is observed experimentally and is also found computationally.

dx.doi.org/10.1021/ja311889v | J. Am. Chem. Soc. 2013, 135, 4743−4756

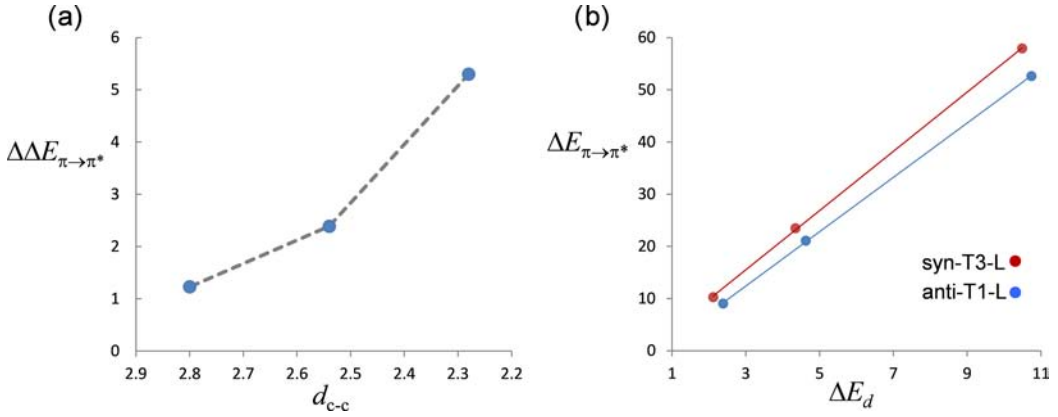

Figure 10. (a) $\Delta\Delta E_{\pi\to\pi^*}$ (kcal/mol) = $\Delta E_{\pi\to\pi^*}$(**syn-T3-L**) − $\Delta E_{\pi\to\pi^*}$(**anti-T1-L**) and is plotted versus d_{c-c} (Å). (b) $\Delta E_{\pi\to\pi^*}$ (kcal/mol) as a function of the distortion energy ΔE_d (kcal/mol).

However, unlike in the electrophilic activation modes, the antiperiplanar transition states are preferred. The preferred transition states have been rationalized using EDA, and the most informative transition-state comparisons (from the data in Tables 2 and 3) are illustrated in Figure 11 for which the remaining conclusions are focused on.

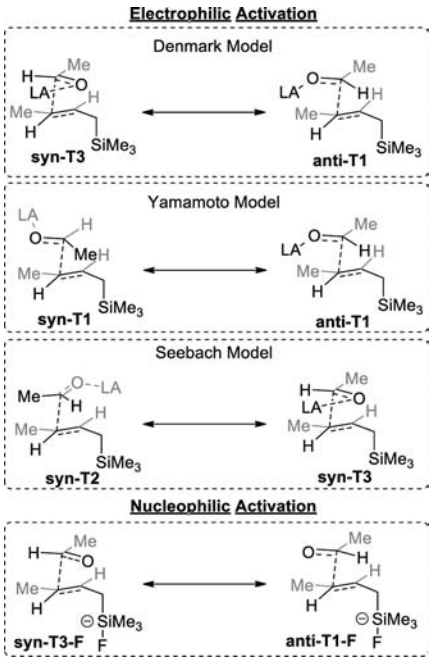

Figure 11. Most relevant transition-state comparisons for crotylation of aldehydes.

5.1. Electrophilic Activation. *5.1.1. Denmark Model.* The observed syn diastereoselectivity in the Lewis acid-promoted pathways primarily arises from the energetic preference for **syn-T3** compared to **anti-T1.** Transition state **syn-T3** is favored electrostatically and through orbital interactions but disfavored sterically relative to **anti-T1**. The preferred orbital interactions for **syn-T3** can be accounted for by favorable orbital overlap conducive to greater charge transfer. The reader should make careful note that these two transition states correspond precisely to the synclinal and antiperiplanar transition states evaluated in the Denmark model system A, Scheme 4. The computationally validated discovery that these two limiting transition states are actually those most relevant to acyclic stereoselection provides a highly satisfying vindication of the significance of that model system. At the time of its disclosure in 1983, the model was heavily criticized as being flawed because it did not compare the synclinal and antiperiplanar transition states that were believed to be relevant in acyclic systems.

5.1.2. Yamamoto Model. The reigning dogma in the field of allylmetal aldehyde additions[6f] posited that the diastereoselectivity could be explained by the difference in energy of the limiting antiperiplanar transition states on the basis of steric considerations (Yamamoto model, Figure 11). The calculated results suggest otherwise as the lower-energy antiperiplanar transition state (**anti-T1**) leads to the anti diastereomer ($\Delta\Delta E^{\ddagger}_{(\text{anti-T1-L}-\text{syn-T1-L})}$ = −3.0 kcal/mol; $\Delta\Delta E^{\ddagger}_{(\text{anti-T1-H}-\text{syn-T1-H})}$ = −1.7 kcal/mol), not the observed syn diastereomer under electrophilic activation. Although the steric contribution to these transition states does indeed favor **syn-T1-L** ($\Delta\Delta E_{\text{exrep}}{}^{\ddagger}_{(\text{syn-T1-L}-\text{anti-T1-L})}$ = −7.8 kcal/mol), this preference does not compensate for the additional contribution from the electrostatic ($\Delta\Delta E_{\text{es}}{}^{\ddagger}_{(\text{anti-T1-L}-\text{syn-T1-L})}$ = −4.4 kcal/mol) and orbital interactions ($\Delta\Delta E_{\text{pol}}{}^{\ddagger}_{(\text{anti-T1-L}-\text{syn-T1-L})}$ = −5.5 kcal/mol) that favor **anti-T1-L**. The origin of the lesser electrostatic and orbital interaction energies for the sterically favored **syn-T1-L** transition state can be ascribed to the greater π-distortion of the crotylsilane component present in **syn-T1-L** similar to that illustrated in Figure 8.[59]

5.1.3. Seeebach Model. According to the empirical rules developed by Seebach (Scheme 2),[1] either the **syn-T2** or the **syn-T3** transition states should be the most favored for these reactions (depending upon whether rule iii or iv is dominant). Interestingly, these two transition states are very close in energy ($\Delta\Delta E^{\ddagger}_{(\text{syn-T3-L}-\text{syn-T2-L})}$ = −0.7 kcal/mol; $\Delta\Delta E^{\ddagger}_{(\text{syn-T3-H}-\text{syn-T2-H})}$ = −1.0 kcal/mol) and are both lower in energy than the lowest-energy transition states leading to the anti diastereomer. The modest preference for **syn-T3-L** arises from the significantly lower steric repulsion energy that more than compensates for slightly less favorable electrostatic and orbital interaction energies.

5.2. Nucleophilic Activation. The observed anti diastereoselectivity in the fluoride-promoted pathway mostly arises from the energetic preference for **anti-T1-F** compared to **syn-T1-F**. The basis for this preference mirrors the analysis for the energetic differences between the antiperiplanar transition states in the electrophilically activated additions. An interesting

dx.doi.org/10.1021/ja311889v | *J. Am. Chem. Soc.* 2013, 135, 4743−4756

comparison can be made between **anti-T1-F** and **syn-T3-F** (Figure 11) because the latter is close in energy to **syn-T1-F** and is favored in both electrophilic activation modes. Whereas synclinal transition structure **syn-T3-F** does exhibit increased orbital interactions, the electrostatic repulsion between the negatively charged oxygen atom and the negatively charged silylmethylene group in **syn-T3-F** offsets the stabilizing effects from increased orbital interactions. Thus, the repulsion in transition state **syn-T3-F** leads to an overall energetic preference for antiperiplanar transition structure **anti-T1-F**. This conclusion is supported by the experimentally observed preference for the **anti-T1-F** transition state in model system A (Scheme 4).

Lastly, the results of this investigation could be extended to the qualitative design or rationalization of systems for the addition of other π-donors including enamines, silyl enol ethers, or silyl ketene acetals, to aldehydes, enones, nitroalkenes or other π-acceptors. Moreover, insight regarding the favorable topology of the reactants in the transition state as well as the factors that control the topology (i.e., steric, electrostatic, or orbital effects) may prove valuable for the design of more stereoselective catalysts for this and similar transformations.

■ ASSOCIATED CONTENT

Supporting Information

Cartesian coordinates, energies, additional reaction pathways, fitted models, bond orders, intrinsic reaction coordinate diagrams, and complete ref 27 are provided. This material is available free of charge via the Internet at http://pubs.acs.org.

■ AUTHOR INFORMATION

Corresponding Author

sdenmark@illinois.edu

Notes

The authors declare no competing financial interest.

■ ACKNOWLEDGMENTS

We are grateful to the National Science Foundation (NSF CHE-1012663 and NSF CHE-1151566). This paper is dedicated to Prof. Dr. Dieter Seebach on the occasion of his 75th birthday.

■ REFERENCES

(1) Seebach, D.; Goliński, J. *Helv. Chim. Acta* **1981**, *64*, 1413−1423.

(2) (a) Heathcock, C. H.; Buse, C. T.; Kleschick, W. A.; Pirrung, M. C.; Sohn, J. E.; Lampe, J. *J. Org. Chem.* **1980**, *45*, 1066−1081. (b) Lam, Y.-H.; Houk, K. N.; Scheffler, U.; Mahrwald, R. *J. Am. Chem. Soc.* **2012**, *134*, 6286−6295.

(3) (a) Rondan, N. G.; Paddon-Row, M. N.; Caramella, P.; Houk, K. N. *J. Am. Chem. Soc.* **1981**, *103*, 2436−2438. (b) Houk, K. N. *Pure Appl. Chem.* **1983**, *55*, 277−282.

(4) Mulzer, J.; Brüntrup, G.; Finke, J.; Zippel, M. *J. Am. Chem. Soc.* **1979**, *101*, 7723−7725.

(5) Schlosser, M. *Bull. Soc. Chim. Fr.* **1971**, 453−459.

(6) Reviews: (a) Sakurai, H. *Pure Appl. Chem.* **1982**, *54*, 1−22. (b) Majetich, G. In *Organic Synthesis: Theory and Applications*; Hudlicky, T., Ed.; JAI Press: Greenwich, CT, 1989; Vol. *1*, p 173−240. (c) Hosomi, A. *Acc. Chem. Res.* **1988**, *21*, 200−206. (d) Schinzer, D. *Synthesis* **1988**, 263−273. (e) Fleming, I.; Dunogués, J.; Smithers, R. *Org. React.* **1989**, *37*, 57−575. (f) Yamamoto, Y.; Asao, N. *Chem. Rev.* **1993**, *93*, 2207−2293. (g) Langkopf, E.; Schinzer, D. *Chem. Rev.* **1995**, *95*, 1375−1408. (h) Masse, C. E.; Panek, J. S. *Chem. Rev.* **1995**, *95*, 1293−1316. (i) Fleming, I.; Barbero, A.; Walter, D. *Chem. Rev.* **1997**, *97*, 2063−2192. (j) Yanagisawa, A. In *Comprehensive Asymmetric Catalysis*; Jacobsen, E. N., Pfaltz, A., Yamamoto, H., Eds.; Springer-Verlag: Berlin, Germany, 1999; Vol. *2*, Chapter 27. (k) Denmark, S. E.; Almstead, N. G. In *Modern Carbonyl Chemistry*, Otera, J., Ed.; Wiley-VCH: Weinheim, Germany, 2000; Chapter 10. (l) Denmark, S. E.; Fu. *J. Chem. Rev.* **2003**, *103*, 2763−2793. (m) Yus, M.; Gonzalez-Gomez, J. C.; Foubelo, F. *Chem. Rev.* **2011**, *111*, 7774−7854.

(7) (a) *Modern Carbonyl Chemistry*; Otera, J., Ed.; Wiley-VCH: Weinheim, Germany, 2000. (b) *Modern Aldol Reactions*; Mahrwald, R., Ed.; Wiley-VCH: Weinheim, Germany, 2004.

(8) For a thorough disquisition on the state of the art in S_E' reactions see: (a) Matassa, V. G.; Jenkins, P. R.; Kümin, A.; Damm, L.; Schreiber, J.; Felix, D.; Zass, E.; Eschenmoser, A. *Isr. J. Chem.* **1989**, *29*, 321−343. (b) Denmark, S. E.; Werner, N. S. *J. Am. Chem. Soc.* **2010**, *132*, 3612−3620. (c) Denmark, S. E.; Weber, E. J.; Almstead, N. G.; Wolf, L. M. *Tetrahedron* **2012**, *68*, 7701−7718.

(9) Reviews: (a) Hoffmann, R. W. In *Stereocontrolled Organic Synthesis*; Trost, B. M., Ed.; Blackwell Scientific Publications: Cambridge; 1994; pp 259−274. (b) Roush, W. R. In *Stereoselective Synthesis, Methods of Organic Chemistry (Houben-Weyl)*; E21; Helmchen, G., Hoffmann, R. W., Mulzer, J., Schaumann, E., Eds.; Thieme Stuttgart: New York, 1996; Vol. *3*; pp 1410−1486. (c) Hall, D. G.; Lachance, H. *Org. React.* **2008**, *73*, 1−573.

(10) (a) Reetz, M. T.; Hüllmann, M.; Massa, W.; Berger, S.; Rademacher, P.; Heymanns, P. *J. Am. Chem. Soc.* **1986**, *108*, 2405−2408. (b) Denmark, S. E.; Henke, B. R.; Weber, E. J. *J. Am. Chem. Soc.* **1987**, *109*, 2512−2514. (c) Shambayati, S.; Crowe, W. E.; Schreiber, S. L. *Angew. Chem., Int. Ed.* **1990**, *29*, 256−272. (d) Ooi, T.; Maruoka, K. In *Modern Carbonyl Chemistry*; Otera, J., Ed.; Wiley-VCH: Weinheim, Germany, 2000; Chapter 1. (e) Saito, S.; Yamamoto, H. In *Modern Carbonyl Chemistry*; Otera, J., Ed.; Wiley-VCH: Weinheim, Germany, 2000; Chapter 2. (f) Denmark, S. E.; Almstead, N. G. *J. Am. Chem. Soc.* **1993**, *115*, 3133−3139.

(11) Denmark, S. E.; Fu, J. *Chem. Commun.* **2003**, 167−170.

(12) (a) Denmark, S. E.; Weber, E. J. *Helv. Chim. Acta* **1983**, *66*, 1655−1660. (b) Denmark, S. E.; Weber, E. J. *J. Am. Chem. Soc.* **1984**, *106*, 7970−7971. (c) Denmark, S. E.; Henke, B. R.; Weber, E. J. *J. Am. Chem. Soc.* **1987**, *109*, 2512−2514. (d) Denmark, S. E.; Weber, E. J.; Wilson, T. M.; Willson, T. M. *Tetrahedron* **1989**, *45*, 1053−1065. (e) Denmark, S. E.; Almstead, N. G. *J. Org. Chem.* **1994**, *59*, 5130−5132. (f) Denmark, S. E.; Hosoi, S. *J. Org. Chem.* **1994**, *59*, 5133−5135. (g) Denmark, S. E.; Almstead, N. G. *J. Mex. Chem. Soc.* **2009**, *53*, 174−192.

(13) Tietze, L. F.; Kinzel, T.; Schmatz, S. *Chem.—Eur. J.* **2009**, *15*, 1706−1712.

(14) Bottoni, A.; Costa, A. L.; Di Tommaso, D.; Rossi, I.; Tagliavini, E. *J. Am. Chem. Soc.* **1997**, *119*, 12131−12135.

(15) Tietze, L. F.; Kinzel, T.; Schmatz, S. *J. Am. Chem. Soc.* **2006**, *128*, 11483−11495.

(16) Morokuma, K. *J. Chem. Phys.* **1971**, *55*, 1236−1235.

(17) Kitaura, K.; Morokuma, K. *Int. J. Quantum Chem.* **1976**, *10*, 325−340.

(18) Su, P.; Li, H. *J. Chem. Phys.* **2009**, *131*, 1−15.

(19) (a) Jeziorski, B.; Moszynski, R.; Szalewicz, K. *Chem. Rev.* **1994**, *94*, 1887−1930. (b) Frenking, G.; Solá, M.; Vyboishchikov, S. F. *J. Organomet. Chem.* **2005**, *690*, 6178−6204.

(20) (a) Bickelhaupt, F. M. *J. Comput. Chem.* **1999**, *20*, 114−128. (b) Diefenbach, A.; Bickelhaupt, F. M. *J. Chem. Phys.* **2001**, *115*, 4030−4040. (c) Diefenbach, A.; Bickelhaupt, F. M. *J. Phys. Chem. A* **2004**, *108*, 8460−8466. (d) de Jong, G. T.; Bickelhaupt, F. M. *ChemPhysChem* **2007**, *8*, 1170−1181. (e) Ess, D. H.; Houk, K. N. *J. Am. Chem. Soc.* **2007**, *129*, 10646−10647. (f) Ess, D. H.; Houk, K. N. *J. Am. Chem. Soc.* **2008**, *130*, 10187−10198. (g) Ess, D. H.; Jones, G. O.; Houk, K. N. *Org. Lett.* **2008**, *10*, 1633−1636. (h) Hayden, A. E.; Houk, K. N. *J. Am. Chem. Soc.* **2009**, *131*, 4084−4089. (i) Ess, D. H. *J. Org. Chem.* **2009**, *74*, 1498−1508. (j) Ess, D. H.; Goddard, W. A., III; Periana, R. A. *Organometallics* **2010**, *29*, 6459−6472. (k) Ess, D. H.; Gunnoe, T. B.; Cundari, T. R.; Goddard, W. A., III; Periana, R. A. *Organometallics* **2010**, *29*, 6801−6815. (l) Devarajan, D.; Ess, D. H. *Inorg. Chem.* **2012**, *51*, 6367−6375.

(21) Mukaiyama, T.; Matsuo, J. In *Modern Aldol Reactions Vol 1: Enolates, Organocatalysis, Biocatalysis and Natural Product Syntesis*, Mahrwald, R., Ed.; Wiley-VCH: Weinheim, Germany, 2004; Chapter 3.
(22) Tomioka, K. In *Modern Carbonyl Chemistry*; Otera, J., Ed.; Wiley-VCH: Weinheim, Germany, 2000; Chapter 12.
(23) Zhao, Y.; Truhlar, D. G. *Theor. Chem. Acc.* **2008**, *120*, 215−241.
(24) Barone, V.; Cossi, M. J. *Phys. Chem. A* **1998**, *102*, 1995−2001.
(25) Ribeiro, R. F.; Marenich, A. V.; Cramer, C. J.; Truhlar, D. G. *J. Phys. Chem. B* **2011**, *115*, 14556−14562.
(26) Alecu, I. M.; Zheng, J.; Zhao, Y.; Truhlar, D. G. *J. Chem. Theory Comput.* **2010**, *6*, 2872−2887.
(27) Frisch, M. J.; Trucks, G. W.; Schlegel, H. B.; Scuseria, G. E.; Robb, M. A.; Cheeseman, J. R.; Scalmani, G.; Barone, V.; Mennucci, B.; Petersson, G. A.; Nakatsuji, H.; et al. *Gaussian 09*, revision A.01; Gaussian, Inc.: Wallingford, CT, 2010.
(28) Schmidt, M. W.; Baldridge, K. K.; Boatz, J. A.; Elbert, S. T.; Gordon, M. S.; Jensen, J. H.; Koseki, S.; Matsunaga, N.; Nguyen, L. A.; Su, S.; Windus, T. L.; Dupuis, M.; Montgomery, J. A. *J. Comput. Chem.* **1993**, *14*, 1347−1363.
(29) (a) Akiyama, T.; Kirino, M. *Chem. Lett.* **1995**, 723−724. (b) Akiyama, T.; Yamanaka, M. *Synlett* **1996**, 1095−1096.
(30) Bottoni, A.; Costa, A. L.; Tommaso, D. D.; Rossi, I.; Tagliavini, E. *J. Am. Chem. Soc.* **1997**, *119*, 12131−12135.
(31) Laurence, C.; Gal, J.-F. *Lewis Basicity and Affinity Scales: Data and Measurement*, John Wiley & Sons: West Sussex, U.K., 2010; Chapter 3.
(32) (a) Reetz, M. T.; Hullmann, M.; Massa, W.; Berger, S.; Rademacher, P.; Heymanns, P. *J. Am. Chem. Soc.* **1986**, *108*, 2405−2408. (b) Denmark, S. E.; Henke, B. R.; Weber, E. *J. Am. Chem. Soc.* **1987**, *109*, 2512−2514. (c) Corey, E. J.; Loh, T.−P.; Sarshar, S.; Azimioara, M. *Tetrahedron Lett.* **1992**, *33*, 6945−6948. (d) Denmark, S. E.; Almstead, N. G. *J. Am. Chem. Soc.* **1993**, *115*, 3133−3139. (e) Ishihara, K.; Gao, Q.; Yamamoto, H. *J. Am. Chem. Soc.* **1993**, *115*, 10412−10413.
(33) Wong, C. T.; Wong, M. W. *J. Org. Chem.* **2007**, *72*, 1425−1430.
(34) Results of the EDA of complex **3** is available in the Supporting Information.
(35) (a) Gerrard, W.; Mooney, E. F.; Peterson, W. G. *J. Inorg. Nucl. Chem.* **1967**, *29*, 943−949. (b) Rasul, G.; Williams, R. E. *Collect. Czech. Chem. Commun.* **1999**, *64*, 847−855.
(36) These pathways and a reproduction of the lowest-energy pathway from the diagram in Figure 1 are available in the Supporting Information.
(37) Computed energy diagram for the $TiCl_4$-promoted pathway is provided in the Supporting Information.
(38) Lee, J. M.; Helquist, P.; Wiest, O. *J. Am. Chem. Soc.* **2012**, *134*, 14973−14981.
(39) System of nomenclature for the transition states used herein designates the following: (1) syn or anti describe the relative topicity of the reacting double bonds in terms of the product stereostructure, (2) T = a transition state, (3) 1 = antiperiplanar, 2 = (+)-synclinal, and 3 = (−)-synclinal arrangement of double bonds; and L = Lewis acid promoted; H = Brønsted acid promoted; and F = fluoride promoted.
(40) See Supporting Information for energy comparisons of geometries of protonated acetaldehyde.
(41) Olah, G. A.; O'Brian, D. H; Calin, M. *J. Am. Chem. Soc.* **1967**, *89*, 3582−3586.
(42) Distortion energy of the aldehyde component is represented as $\Delta E_d(A)$, while the distortion energy of the crotylsilane component is represented as $\Delta E_d(B)$.
(43) Table of computed solvation energies is available in the Supporting Information
(44) All fits contained ≥ 5 points with $R^2 > 0.99$ which are available in the Supporting Information.
(45) Full table of the interaction energy components at the interpolated transition states is available in the Supporting Information.
(46) Corresponding plots are available in the Supporting Information.
(47) Full table of the interaction energy components at the interpolated transition states for all three pathways is available in the Supporting Information.
(48) Whereas **syn-T3-L** and **syn-T3-H** are the lowest-energy pathways, **syn-T3-F** is not the lowest-energy pathway, even though it possesses the strongest orbital interactions (section 4.2.2).
(49) (a) Klopman, G. *J. Am. Chem. Soc.* **1968**, *90*, 223−234. (b) Salem, L. *J. Am. Chem. Soc.* **1968**, *90*, 543−552. (c) Salem, L. *J. Am. Chem. Soc.* **1968**, *90*, 553−566.
(50) Descriptor Δq here is not intended to explain any energetic quantity from the EDA. It is merely illustrated as an additional descriptor to approximate the primary orbital interactions.
(51) This statement is supported by the fact that the orbital interaction energy component (ΔE_{pol}) favors **syn-T3-L** compared to **anti-T1-L** under constant distortion (ΔE_{pol}(**syn-T3-L**) − ΔE_{orb}(**anti-T1-L**) = −5.4 kcal/mol) (Supporting Information).
(52) Anh, N. T.; Thanh, B. T. *Nouv. J. Chim.* **1986**, *10*, 681−683.
(53) Quantities are calculated at constant levels of distortion from Table 2 and in the Supporting Information.
(54) Since the contribution from orbital energy gap is nonexistent from both equalities Δ_x(**syn-T3**) = Δ_x(**anti-T1**) and Δ_x(**anti-T2**) = Δ_x(**syn-T1**) for both electrophilic activation modes, the approach outlined in Figure 7 is acceptable for isolating overlap contributions rather than differences in orbital energy gaps.
(55) Negative values of Δq_L^{SOI} and $\Delta_L^{\mp,SOI}$ and a positive value for ΔE_{pol}^{SOI} indicate greater stabilizing interactions in **anti-T2** which implies the lack of stabilizing SOIs in **syn-T3**. A negative value for ΔE_{int}^{SOI} may indicate a small stabilizing contribution from SOIs.
(56) This additional distortion does not lead to an increase in the HOMO energy of **anti-T2-L** relative to **syn-T3-L**, i.e., the HOMO energies of these transition states are equal. Thus, the lesser distortion in **syn-T3-L** arises from greater orbital overlap rather than a narrowing of the HOMO−LUMO gap.
(57) Bürgi, H. B.; Dunitz, J. D.; Lehn, J. M.; Wipff, G. *Tetrahedron* **1974**, *30*, 1563−1572.
(58) Mayer bonder orders are available in the Supporting Information.
(59) Figure illustrating this distortion difference is available in the Supporting Information.